Journal of Biomedical Optics

SPIEDigitalLibrary.org/jbo

Biospeckle in the human sclera and impact on laser speckle correlation measurement of eye tremor

Emer Kenny
Davis Coakley
Gerard Boyle

SPIE

Biospeckle in the human sclera and impact on laser speckle correlation measurement of eye tremor

Emer Kenny,[a] Davis Coakley,[a] and Gerard Boyle[b]
[a]St. James's Hospital, Mercer's Institute for Research on Ageing, Dublin 8, Ireland
[b]St. James's Hospital, Department of Medical Physics and Bioengineering, Dublin 8, Ireland

Abstract. Ocular microtremor (OMT) is an involuntary fixational eye movement. We identify the implications of biospeckle for a noninvasive, laser speckle correlation technique to measure OMT. Biospeckle from the *in-vivo* eye is characterized and, using the resulting characteristics, a mathematical model to describe the biospeckle from the eye is designed and tested. Through *in-vivo* measurements, biospeckle is shown to disrupt the temporal stability of the speckle images over time. However, provided each speckle image is cross correlated with the previous image within a sufficiently short time, the stability of speckle images captured from the eye is shown to be adequate to measure OMT-like displacements. © *2013 Society of Photo-Optical Instrumentation Engineers (SPIE)* [DOI: 10.1117/1.JBO.18.9.097009]

Keywords: ocular microtremor; speckle metrology; biospeckle; angular speckle displacement; speckle correlation; speckle simulation.

Paper 130452R received Jun. 30, 2013; revised manuscript received Aug. 29, 2013; accepted for publication Sep. 4, 2013; published online Sep. 25, 2013.

1 Introduction

Due to its minute size (12 to 216 μrad peak-to-peak) and rapid oscillation (~84 Hz), ocular microtremor (OMT) is difficult to record accurately. OMT is a fixational eye movement and has been proven to express characteristic changes in a number of clinical conditions.[1–10] To date, the most popular measurement system to record OMT has been an eye-contacting piezoelectric method.[11,12] This contacting technique, however, has many difficulties associated with it, including patient discomfort.[13,14] Ideally, for practical clinical use, OMT would be measured in a noncontact manner.

Noncontact eye-tracking techniques using infrared or video sources have widespread application, including eye tracking as a "pointer" for interactive computer-human display.[15–17] A noncontact laser speckle correlation technique to track and measure angular displacements of the eye in the OMT range has been demonstrated previously using an inanimate surface.[18] The system implements a technique to measure rotational displacement by recording speckle in the Fourier domain of a lens.[19,20] The technical requirements for the system have been outlined and the system was shown to have a dynamic range of 4 to 5000 μrad, a resolution of 4 μrad, and a bandwidth of 250 Hz. In this paper, additional considerations in measuring the angular displacements from the sclera *in-vivo* are presented.

Speckle statistics for inanimate surfaces have been studied extensively[21–25] yet the spatial-temporal statistics of "biospeckle"[26–28] from a biological surface are not so well understood due to their complex nature. A speckle pattern derived from living tissue such as the skin or the eye differs from that observed from an inanimate surface in that the speckles show a spatial-temporal change. Over time, the individual speckles change shape and randomly fluctuate in a manner sometimes referred to as "boiling speckle," so-called due to their resemblance to the boiling of a liquid. The temporal evolution of the speckle is related to physiological changes taking place on and inside the biological surface. These changes cause a variation in the phases of the components of the speckle pattern.

Biospeckle has never been characterized in the human eye. The first objective of the work in this paper is to characterize biospeckle from the human sclera. The second objective is to investigate whether biospeckle image frames captured from the human eye *in vivo* are stable enough to allow displacement of the eye to be measured using speckle correlation.

In this work, speckle patterns from the *in-vivo* sclera are captured using a Fourier plane laser speckle correlation setup. The patterns are characterized using quantitative measures of speckle. The temporal stability of the speckle patterns from the eye is characterized using a measure of frame-to-frame correlation. A mathematical model of the spatio-temporal evolution of speckle patterns from the eye is built. Parameters of the model are set to match the characteristics of the speckle patterns seen *in vivo*. The mathematical model allows simulation of the evolution of the speckle patterns in response to a known input eye tremor movement and simulated level of biospeckle. The ability of a laser speckle correlation technique to recover this movement in the presence of biospeckle is assessed using the mathematical model.

1.1 *Biospeckle in the Eye*

Laser light interaction with biological tissue is complex. The light that penetrates into a surface, such as the eye, is scattered by red blood cells, water, and other tissue. As these scatterers move, the biospeckles created by them move and change shape. The higher the mobility of these scatterers, the higher the expected rate of biospeckle activity.

Here, the interest is in the sclera as the target for a speckle correlation–based eye movement measurement system. The penetration depth of a 632-nm HeNe laser in soft tissue is ~1 to 2 mm,[29] suggesting that the laser light could penetrate beyond the sclera. Each layer of tissue in which the laser

Address all correspondence to: E. Kenny, St. James's Hospital, Mercer's Institute for Research on Ageing, Dublin 8, Ireland. Tel: +353 1 4284882; Fax: +353 1 410 3478; E-mail: kennye3@tcd.ie

0091-3286/2013/$25.00 © 2013 SPIE

light passes through is expected to contribute to the overall activity of biospeckle captured from the sclera.

1.1.1 *Biospeckle characterization*

There is no gold standard metric to describe or measure biospeckle. No single parameter will define biospeckle seen from the sclera *in vivo* and so a multivariate analysis of biospeckle is required.

The following speckle characteristics are commonly found in the literature and can be used to describe biospeckle patterns: grey level histogram, speckle contrast, time history speckle pattern (THSP),[27] grey level co-occurrence matrix (GLCM)[30] and the moment of inertia (IM).[31]

In this work, three other statistics derived from the GLCM and typically used for texture analysis,[30] will also be implemented to describe the speckle images. These are the energy, homogeneity, and correlation of the GLCM. Correlation is a measure of how a pixel is correlated to its neighbour. Homogeneity returns a value that measures the closeness of the distribution of elements in the GLCM to the GLCM diagonal. Energy returns the sum of squared pixel values of the GLCM and is equal to unity for a constant image.

1.2 *Speckle Correlation Metrology*

The setup for speckle correlation metrology is shown in Fig. 1. Light from a collimated, plane-polarized laser beam is directed through a beam splitter to a target where it is then reflected back to an image sensor placed in the Fourier plane (i.e., $z_2 = f$) of a lens with aperture σ. The out-of-plane angular rotation (θ) of the object is transformed to a linear displacement in the Fourier plane of a lens. An image sensor placed in the Fourier plane records the speckle patterns over a certain time.

During postprocessing, the recorded speckle image frames are compared using a cross-correlation algorithm. The location of the cross-correlation peak between a reference frame and a shifted "test" frame shows the displacement shift, in pixels, between the two images. Using known parameters of the optical setup, this shift is converted from pixels to units of angular rotation, i.e., radians.

The cross-correlation algorithm used for digital speckle correlation detects both the cross-correlation peak location and the peak height. It is important for the success of the speckle correlation technique that the peak location be measured correctly and accurately. In order to measure displacement using the proposed speckle correlation technique, it is essential that the speckle pattern of the reference image frame and the k'th frame remains correlated.

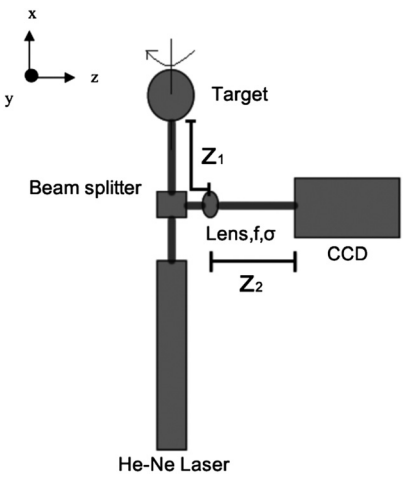

Fig. 1 Set-up for speckle correlation.

Large movements between two imaged speckle patterns result in decorrelation. The decorrelation can also occur due to changes in the speckle pattern triggered by biospeckle. It is expected that other fixational eye movements (drift and microsaccades) and particularly biospeckle will cause decorrelation between image frames captured from the sclera. It may be necessary to acquire a new reference image frame at intermittent intervals to maintain correlation stability between the current and reference frame.

1.2.1 *Frame stability*

For cross-correlation displacement tracking to be successful, it is desirable that the correlation peak be sharp and large so that it is distinguishable from background. A sharp peak indicates a good match between images. As image frames become more decorrelated, the height of the cross-correlation peak drops and the width of the peak becomes broader. To quantify this feature, a peak height-to-floor ratio, analogous to a signal-to-noise ratio, can be used. To calculate this ratio, the peak value of the cross-correlation plot is determined and then divided by the average of the background floor value. The decibel value of the peak-to-floor ratio was calculated as

$$\text{Ratio} = 20\,\log\left(\frac{\text{Peak Value}}{\text{Mean Floor}}\right). \tag{1}$$

A high peak height-to-floor ratio indicates better noise (biospeckle) tolerance and a lower probability of error in the measurement results.

1.3 *Volume Scattering*

The scattering that produces speckle can originate either from the surface of an object or within the object's volume.[32] Volume scattering occurs when light penetrates a surface and undergoes multiple scattering before emerging from the surface. In cases of volume scattering, a component of surface scattering also exists. Speckle patterns from a material into which light penetrates are composed of different sized speckle: (1) large speckles originating from light scattered from the surface and (2) smaller speckles produced by light emerging from the inner volume of the material.[33]

The performance of the proposed speckle correlation system was previously tested and verified using an approximately single scattering surface.[18] A single scattering surface is a simplified model of what is expected *in vivo*. In an *in-vivo* situation, which features the eye sclera as a target for laser light, the laser light is expected to be multiply scattered by the scleral tissue.

The theory of speckle metrology for speckle generated by volume scattering is less developed than that for surface scattering and the influence of volume scattering might have on speckle correlation is yet to be determined.

1.4 *Mathematical Biospeckle Simulation*

To simulate the effects of biospeckle, a phase variance model[28,34,35] is followed in this work. In the model, random phase variations are included into the speckle matrix of each generated speckle pattern to simulate the phase change caused by the scattering centers in living objects that lead to biospeckle.

Using the model, a scattering center has a phase distribution $\phi(m,n,k)$, given by[28]

$$\phi(m,n,k)=\phi(m,n,k-1)+G(m,n,k)\sigma[\Delta\phi(k-1,k)], \quad (2)$$

where $\sigma[\Delta\phi(k-1,k)]$ is the standard deviation of the phase changes between frame $k-1$ and frame k. k varies from 1 to $K-1$, where K is the total number of frames. G is a random $N\times N$ matrix with a Gaussian distribution with a mean of zero and a standard deviation of unity.[35] A new random matrix for G_k is calculated for every frame in the speckle sequence. The degree of biospeckle is related to the magnitude of the phase changes between subsequent frames, i.e., a large phase difference between speckle frames is equivalent to a high degree of biospeckle. Hence, the larger the value of $\sigma[\Delta\phi(k-1,k)]$, the more biospeckle that is present in a speckle pattern. Assuming that a constant "level" of biospeckle is present in a given simulation, then $\sigma[\Delta\phi(k-1,k)]$ reduces to the same value $\sigma[\Delta\phi]$ between each frame.

It should be noted that the above model assumes no other form of speckle displacement is taking place. If the speckle pattern was not stationary, the correlation coefficient would be reduced due to the speckle displacement as well as due to the presence of any biospeckle.

2 Methods

2.1 *In vivo*

The optical setup for the *in-vivo* experiment is illustrated in Fig. 2. *In-vivo* speckle measurements were captured from three healthy volunteers. The volunteers (three healthy females, mean age of 28 years) were instructed to maintain a steady head position while a recording was taken from the sclera of their right eye. Written informed consent was obtained from the volunteers and the protocol was approved by the local ethics committee (St. James's/AMNCH Research Ethics Committee).

The sclera of the volunteers was illuminated by a 632.8-nm plane polarized HeNe laser which was reduced down to an eye-safe power of 180 μW, for an exposure duration of 10 s, by the use of a neutral density filter and a beam splitter. The speckle pattern generated on the sclera target was collected by an EMCCD camera (Cascade 128+, Roper Scientific, Arizona[36]) operating at 500 Hz with a 128×128 array of 24-μm pixels and a 100% fill factor. The EMCCD sensor was placed in the Fourier plane of a lens with a focal length of 150 mm. A 5 s (2500 frames) reading was taken for each measurement. The 8-bit, uncompressed, digitized speckle image frames were then sent to the numerical software package MATLAB[37] for processing.

2.1.1 *In-vitro comparison*

An OMT simulator device[18] with an inanimate cardboard surface was used so that the level of stability achievable with biospeckle could be compared to that of a nonbiological reference. The procedure above was repeated using the OMT simulator.

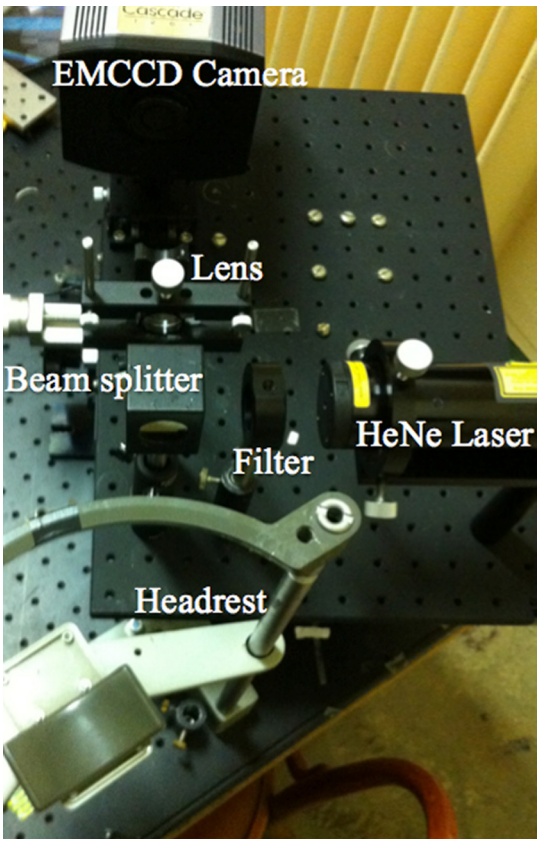

Fig. 2 Experimental setup for *in vivo* measurement.

Note that the "simulator" is a physical device used to test the measurement system, whereas the "simulation," described elsewhere in this paper, is a mathematical model of eye tremor and biospeckle. The simulator replicates OMT movement in terms of typical frequencies and amplitudes. A cardboard target was attached to the simulator surface and the simulator was set at 80 Hz and 4 μrad peak-to-peak. The amplitude of 4 μrad was chosen to test the stability, as it is the lowest amplitude that could be tested using the simulator.

2.1.2 *Biospeckle characterization*

The speckle patterns recorded from volunteers *in vivo* were quantified using the parameters THSP, GLCM, IM, energy, homogeneity, and correlation of GLCM. The mean values of the *in-vivo* results were then compared to the values found for the mathematically simulated biospeckle frames.

2.1.3 *Frame stability*

The peak height-to-floor ratio was analyzed for each of the *in-vivo* speckle videos from the volunteers and for the simulator speckle images. The mean floor value of the correlation plot was calculated, excluding a 10×10 pixel mask around the correlation peak. This area was omitted since it may contain a part of the peak.

Setting the first frame as the reference frame, a log plot of $y=20$ log (peak value/mean floor) for the correlation of each subsequent frame with the reference frame was plotted.

Data from the *in-vivo* sclera biospeckle frames, collected from all three volunteers, were next used to establish how rapidly the speckle frames decorrelate. First, each frame (k) of the

2500 biospeckle images was correlated with the previous frame $(k-1)$, and the average peak height-to-floor ratio was calculated. The procedure was then repeated for correlation of frame (k) with frame $(k-n)$, where n ranged from 2 to 10. In total, comparisons were made for delays ranging from 2 to 20 ms.

2.2 *Simulated Biospeckle*

To simulate the biospeckle patterns seen *in vivo*, a numerical model was generated in MATLAB. In the model, we assume the speckle pattern intensity at the detector, $I(x,y)$, arises from interference of speckles generated from surface scattering and speckles generated from volume scattering. The surface scattering component was taken to shift on the detector in response to rotation of the target. The volume scattering component, however, was assumed to remain unchanged with displacement. Both components accumulated random phase errors with time due to biospeckle effects.

An $S_n(x,y)$ matrix, signifying complex speckle amplitudes, was created to represent surface speckle and had a larger inputted speckle size, $\sigma_s = 2$ pixels. The matrix $V_k(x,y)$, also signifying complex speckle amplitudes, was made to represent volume scattering and was given a smaller input speckle size, $\sigma_v = 0.8$ pixels. These speckle size values were chosen empirically so that the speckle size of the final simulated biospeckle image matched the speckle size seen *in vivo*.

The value of the standard deviation of the phase difference between each generated speckle frame, $\sigma\Delta\phi$, was altered experimentally until it produced speckle that resembled the speckle patterns seen *in vivo*.

Mathematical speckle was generated by adopting speckle simulation methods outlined by Goodman,[32] Duncan and Kirkpatrick,[38] and Rabal and Braga.[28] The process that was used to model biospeckle is illustrated in Fig. 3 and outlined below:

1. In the first iteration of the code $(k = 1)$, the phase matrix, $\phi(m,n)$, is a random 128×128 uniform phase distribution between 0 and 2π as performed in the speckle generation steps by Duncan and Kirkpatrick.[38] After the first iteration, the phase matrices ϕ_k were created in accordance with Eq. (2) by multiplying $\sigma\Delta\phi$ with a matrix of random numbers, G_k and adding the product to the previous phase matrices ϕ_{k-1}.
2. The phase matrices were zero padded in matrices $s_k(x,y)$ and $v_k(x,y)$ of size $M \times M$ and $P \times P$, respectively, where $M = \sigma_s \times 128$ and $P = \sigma_v \times 128$.
3. A fast Fourier transform was performed on both $s_k(x,y)$ and $v_k(x,y)$ to yield arrays representing the complex amplitude speckle at the detector, i.e., to create $S_k(x,y)$ and $V_k(x,y)$.
4. To replicate the displacement of the speckle pattern caused by surface movements, the data in the $S_k(x,y)$ matrix was displaced using the Fourier shift theorem.

   To account for the volume scattering effects of the sclera, the $V_k(x,y)$ matrix was multiplied by a multiple scattering amplitude factor (MSAF). The MSAF is a measure of the relative amplitude of the surface and volume component of scattering. Here, the MSAF factor was set to 0.5.
5. The two matrices were added together on a complex basis, resulting in the matrix $T_k(x,y)$.
6. The matrix $T_k(x,y)$ was multiplied by its complex conjugate $T_k * (x,y)$. In accordance with the speckle generation method used by Duncan and Kirkpatrick,[38] the $M \times M$ and $P \times P$ matrices were low pass filtered by resizing them to the desired array size, 128×128 pixels. This created the first biospeckle intensity image frame $I_{k=1}(x,y)$.
7. The process was repeated until the desired number of image frames, K, was created.

To simulate the effect of eye movement on the speckle pattern, a 5-s long fixational eye movement trace that had been previously acquired *in vivo* using a piezoelectric (PZT) probe system[39,40] was used to drive the speckle pattern displacement in the simulation. The trace was the raw output of the PZT probes and included drift and microsaccades. This introduced a known movement into the simulation. With a simulated sampling frequency of 500 Hz, a total of 2500 speckle frames were generated over the duration of the movement.

2.2.1 *Verification of OMT Signal Recovery from Cross Correlation*

The mathematically generated speckle frames were used to determine the ability of the speckle correlation algorithm to

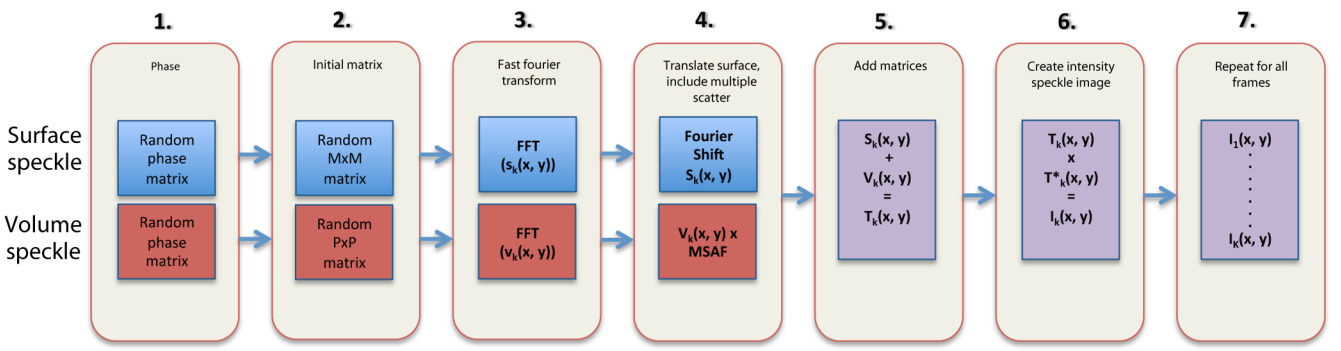

Fig. 3 Biospeckle simulation procedure.

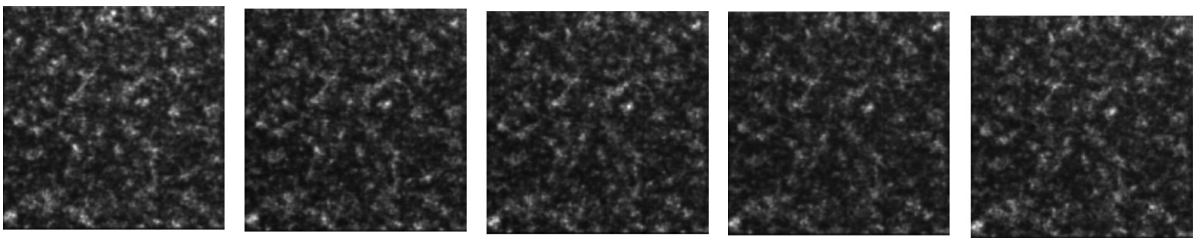

Fig. 4 Five sequential frames taken *in vivo* from the sclera, 2 ms apart.

extract the known OMT movement in the presence of simulated biospeckle. After the speckle frames were generated and displaced, they were further processed in MATLAB. The analysis procedure to calculate the angular speckle displacement from the cross-correlation peak has been described previously.[18] The displacement trace recovered from the simulation was then compared to the displacement trace inputted to the simulation from the OMT-PZT measurement system recording.

3 Results

3.1 *In vivo*

Figure 4 shows five sequential speckle frames taken 2 ms apart from the sclera of one volunteer. An initial qualitative analysis of the frames indicates similar features in each frame and they appear reasonably stable at this frame interval. The speckle size for the example shown was found to be 80 μrad (1 pixel).

3.1.1 *Biospeckle characterization*

The results of the *in-vivo* speckle characterization are presented alongside those of the simulated biospeckle patterns for comparison purposes.

3.1.2 *Frame stability*

Figure 5(a) shows a cross-correlation plot calculated between two speckle frames taken 5 s apart, using the speckle collected from the simulator with cardboard surface while it was running at 80 Hz, 4 μrad peak-to-peak. Figure 4(b) shows the cross-correlation plot for the same recording, however, each frame was correlated with the previous frame and the frames used to generate the correlation plot were taken 2 ms apart. Figures 5(c) and 5(d) show typical *in-vivo* cross-correlation plots created using frames captured at 5 s and 2 ms apart.

Both the plots generated using speckle from the simulator show a clear cross-correlation peak. This demonstrates that even at a very low amplitude (4 μrad) and a time difference of 5 s, the speckle correlation algorithm can measure the displacement of an inanimate object.

In Fig. 5(c), the peak of the correlation plot for the *in-vivo* biospeckle is indistinguishable from background. This shows that the biospeckle frames become completely decorrelated when they are cross-correlated 5 s apart. The decorrelation is due to temporal changes caused by a combination of actual eye movement, biospeckle, and the low contrast associated with the collected images. In the case where each frame is correlated with the previous frame (2 ms apart), the correlation peak for the *in-vivo* speckle images is more distinguishable, less noisy, and larger.

Figure 6 shows the results of measuring the peak height-to-floor ratio over time for (1) the simulator at 80 Hz, 4 μrad peak-to-peak with each frame correlated to the first, reference frame (2) the simulator at 80 Hz, 4 μrad peak-to-peak with each frame correlated to the previous frame (time between frames: 2 ms) (3) one subject's sclera with each frame correlated to the first, reference frame, and (4) the same volunteer's sclera with each frame correlated to the previous frame.

As shown in the figure, in the *in-vivo* case when each frame is correlated with the previous frame, the peak height-to-floor ratio amplitude is higher than that for each frame correlated with the original reference frame. The simulator results show almost constant correlation peak amplitude with time when correlated with the previous frame or when correlated with the first frame.

The poor amplitude of the *in-vivo* result derived from each frame being correlated with the original reference frame is a consequence of biospeckle acting as noise. Biospeckle causes subsequent speckle images to become progressively more different. When each frame is correlated with the previous frame, the image pairs are relatively similar across the tested range. Each frame correlated with the previous frame gave a mean correlation peak-to-floor ratio of 0.19 dB, and an increase of 0.16 dB compared to correlation with an original reference frame.

Figure 7 shows the dependence of the mean correlation peak height-to-floor ratio on the number of frames between the reference frame and the tested frame *in vivo* for three different volunteers. As can be seen in the figure, the frames decorrelated rapidly. When the frames were correlated with a reference frame, five frames proceeding it (a time difference of 10 ms), the peak height amplitude dropped to a value <0.1 dB. In comparison, for the inanimate cardboard surface, absence of biospeckle, the peak height-to-floor ratio never dropped lower than 0.97 dB. This demonstrates that the decorrelation effects in the eye occur rapidly.

3.2 *Simulated Speckle*

3.2.1 *Biospeckle characterization*

The speckle size of the *in-vivo* speckle images was calculated from the full-width half-maximum to be 1 pixel. Using speckle sizes of $\sigma_s = 2$ pixels and $\sigma_v = 0.8$ pixels, the speckle size seen *in vivo* was replicated in the simulated biospeckle images. The standard deviation of the phase difference between speckle frames, $\sigma(\Delta\phi)$, was found to provide the closest resemblance to the biospeckle seen *in vivo* when $\sigma(\Delta\phi)$ was set equal to 0.11 rad between frames separated by 2 ms.

An *in-vivo* speckle image recorded from one volunteer and a mathematically generated speckle image are shown in Fig. 8. The image histograms of all frames from the *in-vivo* and simulated speckle sequence are shown alongside the speckle images. As evidenced, the simulated and *in-vivo* images appear similar in terms of the speckle size and distribution. Likewise, the

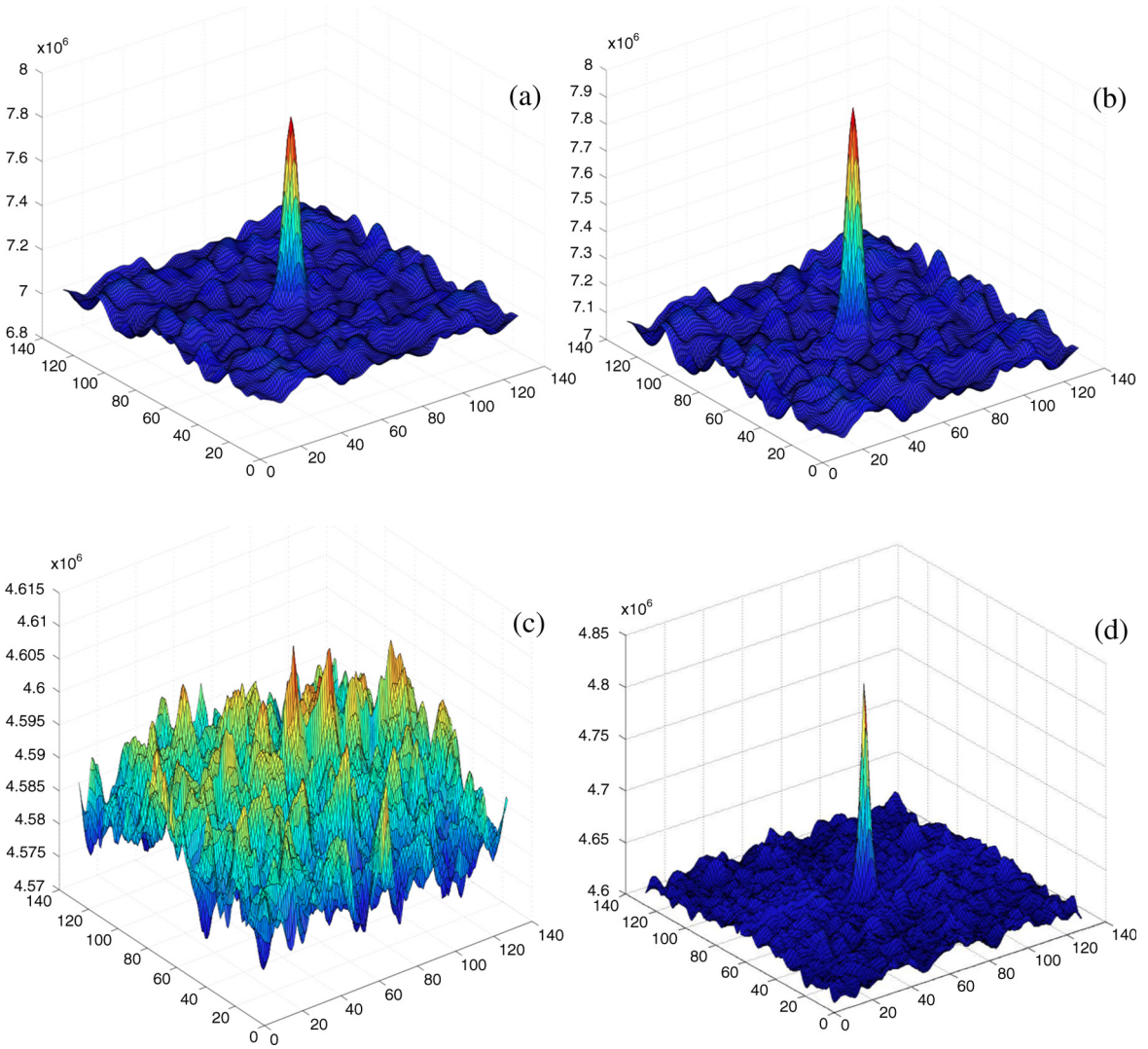

Fig. 5 Cross-correlation plots for (a) speckle frames recorded at 5 s apart on the simulator running at 80 Hz, 4 μrad peak-peak (b) frames recorded at 2 ms apart on the simulator running at 80 Hz, 4 μrad peak-peak (c) frames recorded at 5 s apart *in vivo* and (d) frames recorded at 2 ms apart *in vivo*.

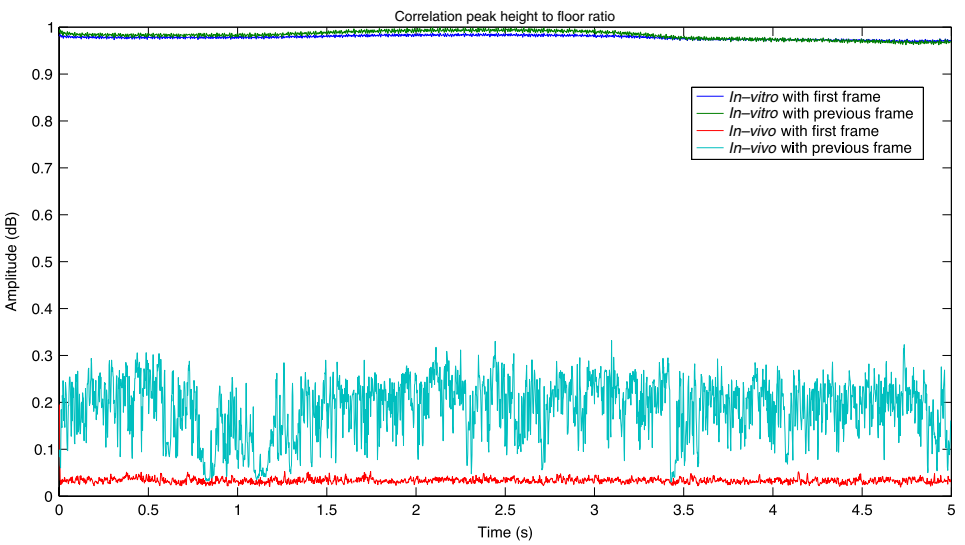

Fig. 6 Correlation peak height-to-floor ratio plotted against time for *in-vitro* speckle frames and for *in-vivo* speckle frames for a single subject.

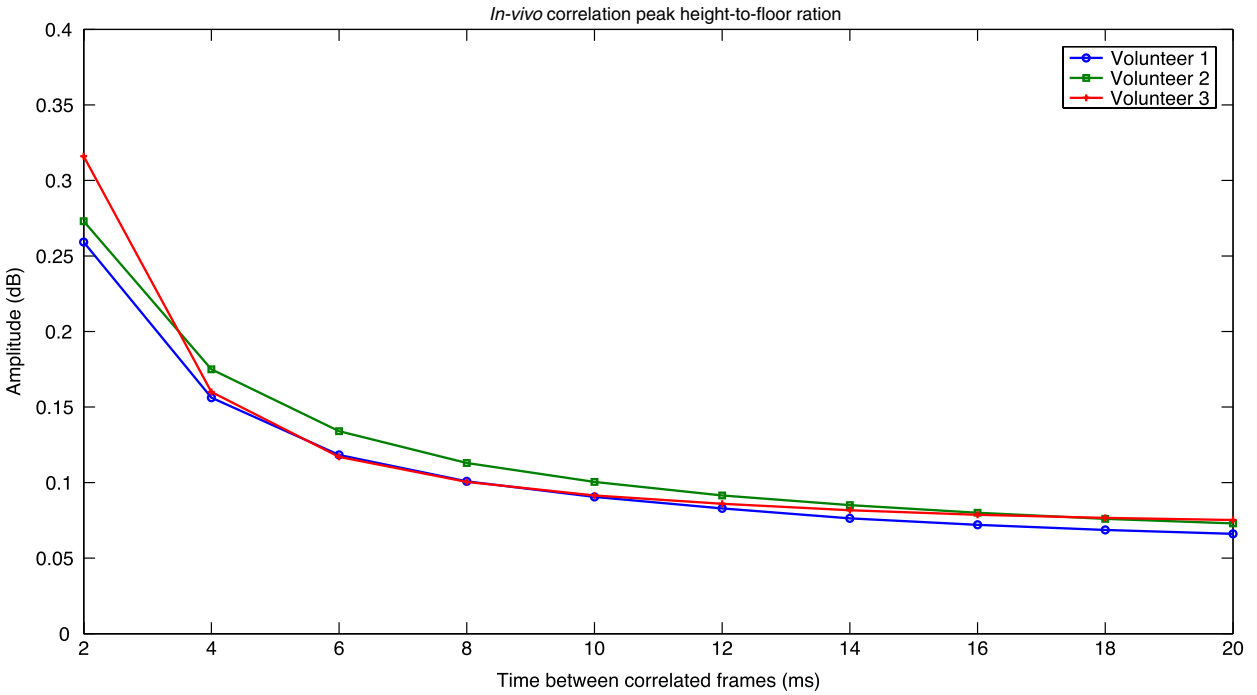

Fig. 7 Dependence of peak height-to-floor amplitude on the time between the reference frame and the tested frame. Frames were recorded at 2 ms apart and the values shown are mean values as measured over 5 s.

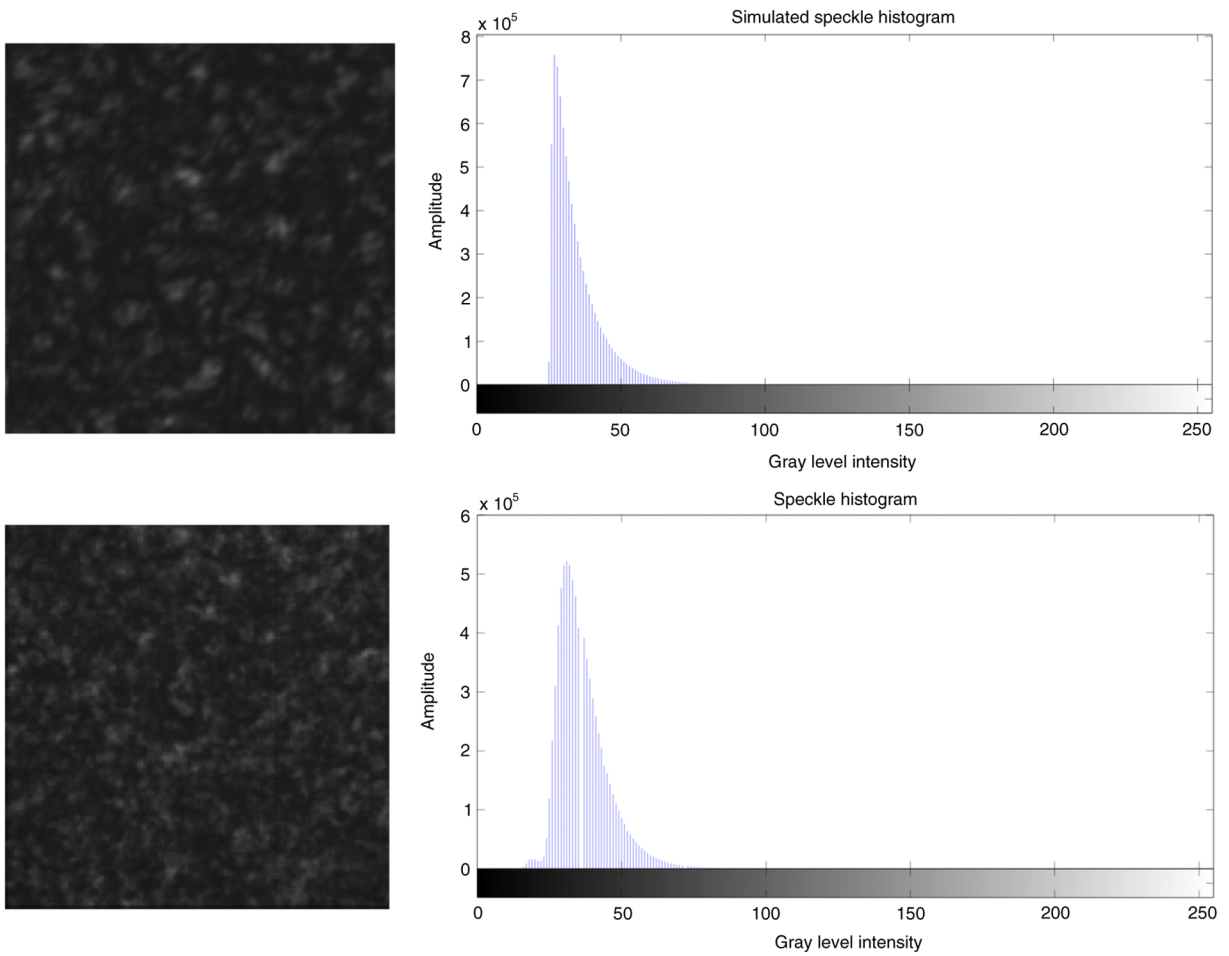

Fig. 8 Simulated biospeckle pattern and the histogram created from all frames in the series (top) and biospeckle from *in-vivo* eye sclera and the histogram created from all frames in the series (bottom).

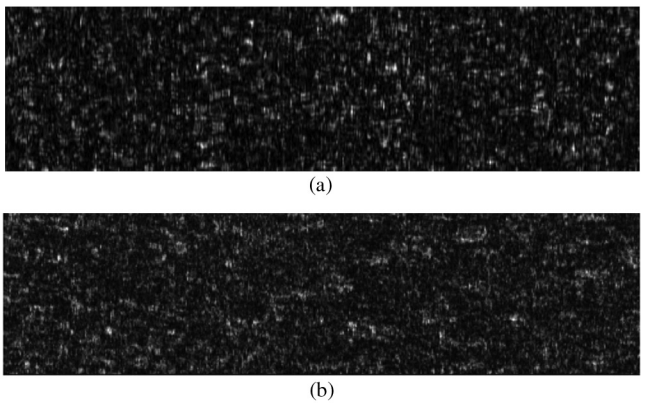

Fig. 9 Time history speckle pattern (THSP) from simulated speckle (a) and from *in-vivo* eye (b).

histograms display similar features in terms of the spread of gray values, shape of the histogram, and histogram skewness.

Figures 9 and 10 show the THSPs and GLCM derived from the *in-vivo* and from the simulated biospeckle image sequences. Qualitatively, the THSPs and GLCMs appear comparable, displaying a high biospeckle activity through a fast change in pixel intensity over time.

Table 1 shows the quantitative results of the second-order statistics calculated from the GLCM of the THSP for (1) volunteers *in vivo* and (2) a series of simulated speckle patterns ($\sigma_s = 2$ pixels, $\sigma_v = 0.8$ pixel) with variable biospeckle levels. The rationale for a choice of biospeckle level set at $\sigma(\Delta\phi) = 0.11$ rad can be seen from Table 1 as this value gives a reasonable match between all observed and simulated parameters.

As expected, the mean stability of the images decreased with increasing $\sigma(\Delta\phi)$. The correlation parameter, derived from the GLCM, showed a notable variation in the simulation as $\sigma(\Delta\phi)$ increased. The IM increased as the $\sigma(\Delta\phi)$ increased, this was to be expected since a higher IM is indicative of higher biospeckle activity. The energy and homogeneity showed a slight change as $\sigma(\Delta\phi)$ changed.

To measure the similarity between the inputted PZT signal and the measured output signal for the speckle simulations, a signal cross-correlation was performed.[41]

The results are shown in Table 1 and a plot of the mean correlation peak height-to-floor ratio against input and output signal cross-correlation is shown in Fig. 11. The cross correlation used here is insensitive to scaling but is influenced by signal shifting. The cross correlation never reached the maximum value of unity. This is likely to be in part due to signal shifting and part due to actual differences in the input and simulated output signals. The

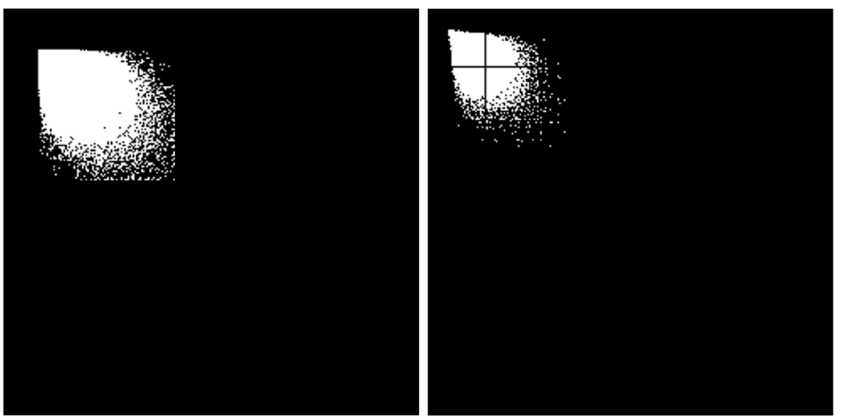

Fig. 10 Gray level co-occurrence matrix (GLCM) from simulated biospeckle (a) and from *in-vivo* eye (b).

Table 1 *In-vivo* parameters of biospeckle and change in simulated biospeckle parameters with increasing phase change. $\sigma\Delta\phi = 0.11$ was the chosen value used in simulations. Multiple scattering amplitude factor (MSAF) was equal to 0.5 for simulated speckle. The time between frames was 2 ms.

		Phase change, $\sigma\Delta\phi$ (rad)											
	In vivo	0	0.03	0.05	0.07	0.09	0.11	0.13	0.15	0.17	0.19	0.21	0.23
Mean peak height-to-floor ratio (dB)	0.28 ± 0.03	0.58	0.5	0.47	0.43	0.38	0.32	0.27	0.22	0.17	0.13	0.09	0.07
Moment of inertia (IM)	61.94 ± 17.78	18	19	27	41	52	65	80	93	106	116	122	132
Correlation	0.63 ± 0.10	0.89	0.87	0.81	0.74	0.64	0.55	0.45	0.36	0.28	0.22	0.16	0.11
Energy	0.003 ± 0.001	0.011	0.007	0.006	0.005	0.004	0.004	0.004	0.003	0.003	0.003	0.003	0.003
Homogeneity	0.29 ± 0.02	0.54	0.44	0.39	0.34	0.31	0.29	0.27	0.26	0.25	0.24	0.24	0.23
Signal correlation	N/A	0.53	0.53	0.53	0.54	0.53	0.53	0.54	0.54	0.54	0.32	0.06	–0.03

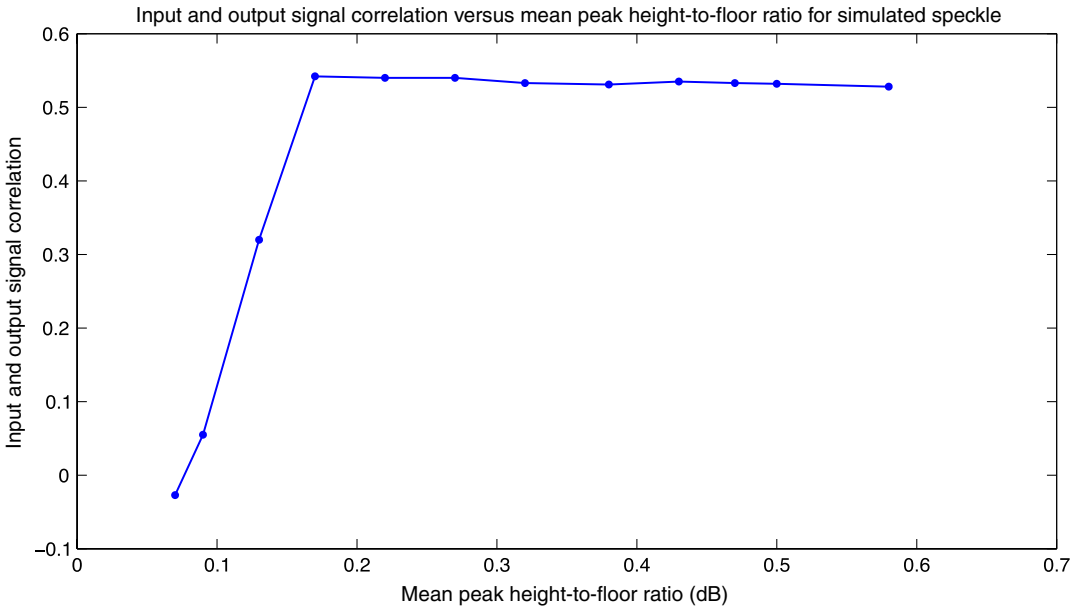

Fig. 11 Mean peak height-to-floor ratio against input and output signal cross-correlation for simulated speckle images.

signal cross correlation decreased drastically after the correlation peak height-to-floor ratio amplitude fell <0.1 dB. This level of stability sets a lower limit on how stable the biospeckle images need to be to measure OMT displacement.

3.2.2 *Simulated frame stability*

Using the same procedure outlined in Sec. 2.1.3 for *in-vivo* speckle images, the stability of the simulated biospeckle image frames was tested over time. To imitate the *in-vivo* experiment, the simulation was repeated three times with different random speckle realizations. Figure 12 displays the dependence of the correlation peak height-to-floor ratio on the time between correlated frames for both the mean of the *in-vivo* results and the mean of the simulated results. As can be seen from the plot, the two cases show similar decaying curves, however, the simulated results have a faster drop in peak height amplitude and fall <0.1 dB after 6 ms.

3.2.3 *Verification of OMT signal recovery from cross correlation*

Figure 13 displays both a filtered version of the PZT trace inputted to translate the simulated biospeckle patterns and the

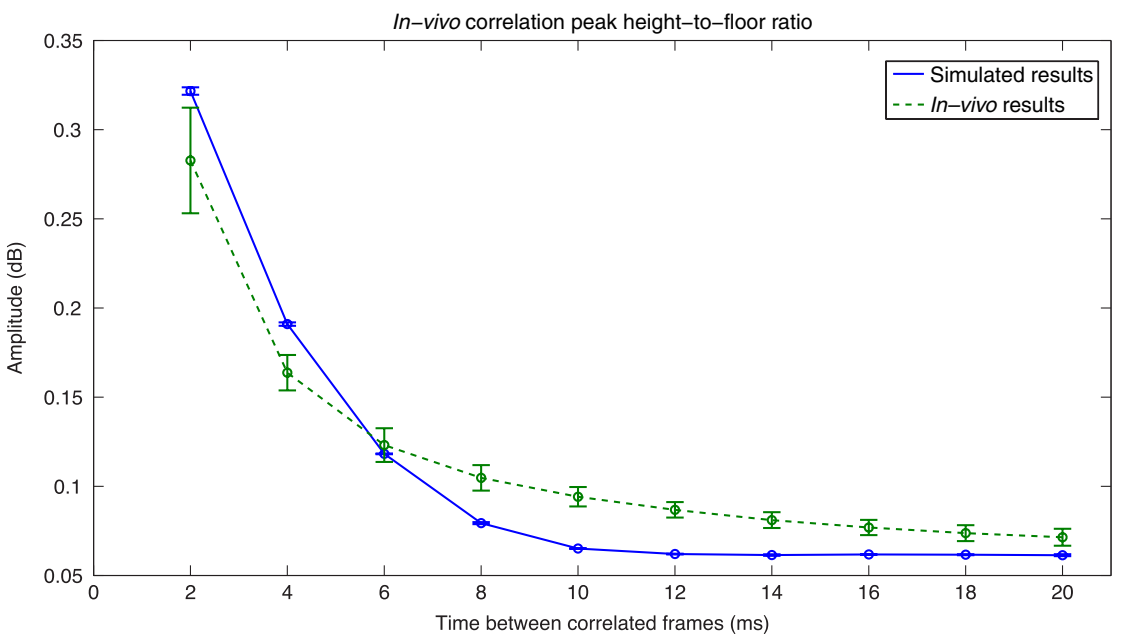

Fig. 12 Dependence of the peak height amplitude on time between the reference frame and the tested frame. The solid line represents the mean of the simulated results, whereas the dashed line represents the mean of the *in-vivo* results. Frames were recorded at 2 ms apart and the values shown are measured over 5 s.

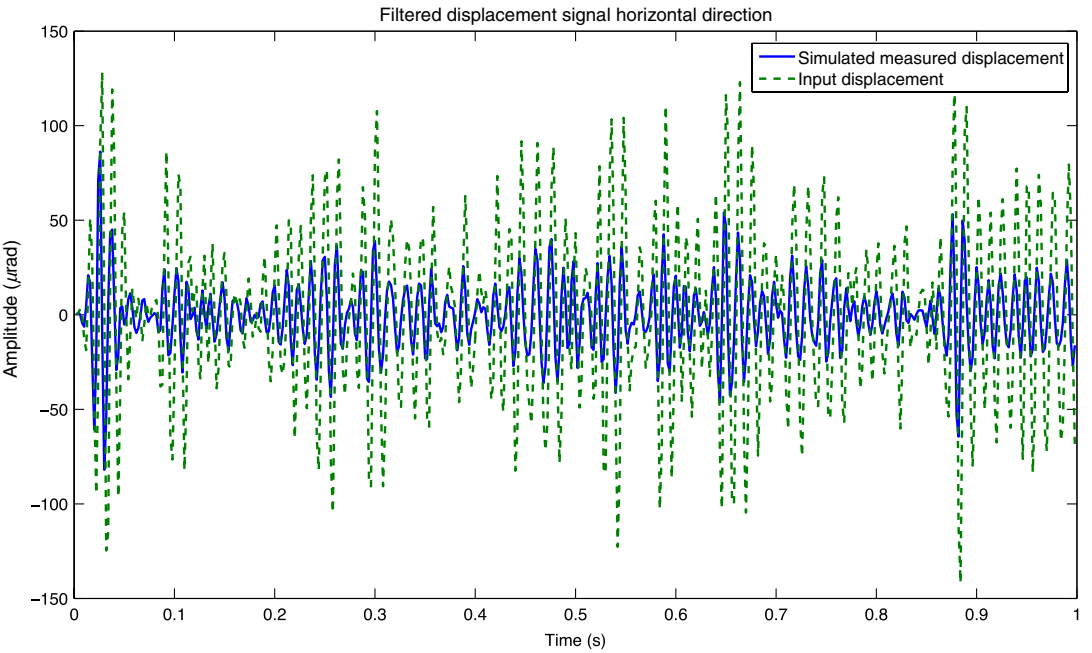

Fig. 13 Filtered input data (dashed line) and filtered displacement recovered from simulated speckle images (solid line).

simulated filtered measured displacement's trace using speckle correlation. Filtering was performed using a Butterworth band-pass filter between 20 and 150 Hz. The speckle patterns in the simulation were created using the same parameters that generated the patterns and results seen in Sec. 3.2.1. The time between each frame was 2 ms. The measured result was found to underestimate the amplitude by 51%. However, importantly, it was capable of tracking the displacement and recreating the general shape of the OMT trace.

Another simulation of the measurements was performed but with MSAF set to zero. The modeled case was equivalent to a surface scattering surface showing biospeckle but no volume scattering.

Figure 14 displays the input and measured displacements for the simulated speckle with MSAF set to zero. As shown in the plot, the measured displacement was in good agreement with the input displacement. A measurement error of only 1% was calculated. These results show that time-varying biospeckle alone does not disrupt the measurements at short frame-to-frame intervals, however, when a multiple scattering field is introduced, it causes systematic underestimation of amplitude.

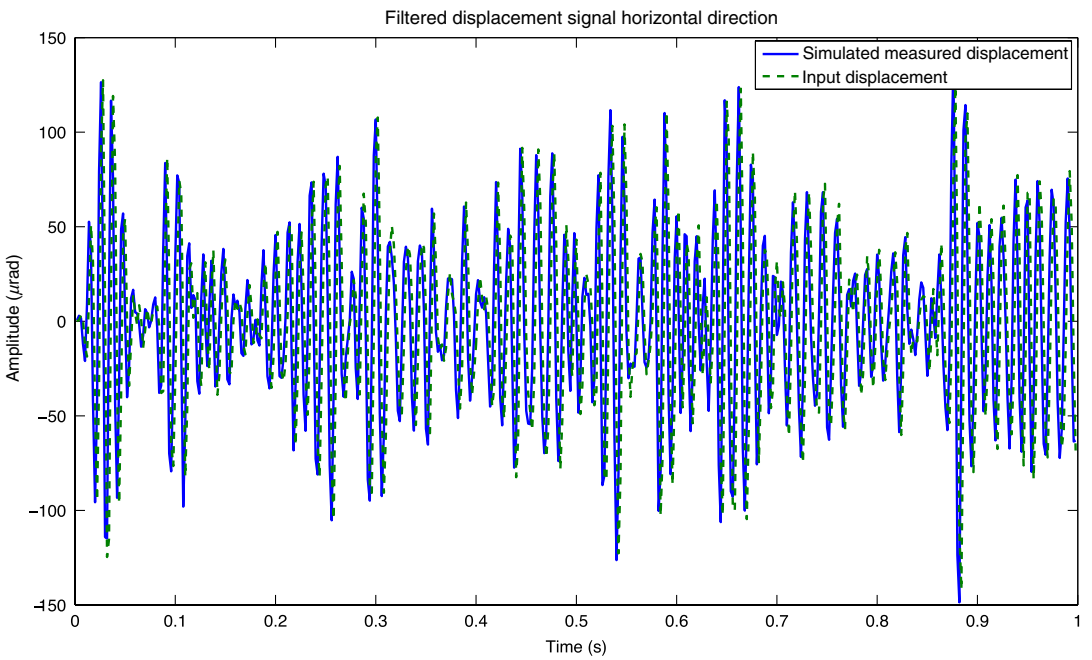

Fig. 14 Filtered input data (green) and filtered displacement recovered from simulated biospeckle images (blue). Multiple scattering amplitude factor (MSAF) was equal to zero.

4 Discussion

The aim of this work was to determine if *in-vivo* biospeckle images captured from the human sclera are sufficiently stable for speckle cross-correlation displacement tracking to be used for eye movement measurement and, in particular, for OMT measurement. The stability of the biospeckle images was investigated using metrics to characterize the correlation peak between frames.

In this work, *in-vivo* speckle images were seen to become unstable rapidly. After five frames (10 ms), the correlation peak height-to-floor ratio was found to drop <0.1 dB. A question arises as to whether this decorrelation is due to biospeckle or perhaps due to movement. Certainly, no significant decorrelation was seen here from an inanimate surface moving at OMT amplitudes. In a real eye, other movements are also at play. The maximum possible displacement of the sclera due to normal eye movement at a frame rate of 500 fps is estimated to be 1.56 mrad/frames. With the same optical configuration used here, the results of previous work[18] using our proposed system on an inanimate diffuse object with a near ideal speckle surface found that the speckle cross-correlation technique broke down at a displacement of about 5 mrad. It seems reasonable to suggest that the dominant effect causing decorrelation between frames taken at brief intervals apart is in fact biospeckle.

To obtain the highest correlation peak *in-vivo* and keep decorrelation at a minimum, the time period between frame correlation needs to be short. In effect, this means tracking displacement using a frame-to-frame correlation rather than a reference frame. A drawback of this method is that as the displacement trace is generated by integrating all frame-to-frame displacements, and any error that occurs during one correlation pair builds in to the displacement result and the error accumulates.

Biospeckle-induced changes in a speckle pattern were numerically simulated in this work by creating a series of speckle matrices whose phase changes between speckle image frames. The simulated speckle images were shown to be qualitatively comparable to those found *in vivo* and a quantitative analysis of metrics derived from the GLCM also provided similar results. An OMT signal, previously recorded using a PZT system, was used to translate the simulated speckle images. We modeled biospeckle as a simple accumulation of phase errors from frame-to-frame. Using this approach, the predicted and actual fall off in frame-to-frame correlation (as quantified using the peak height-to-floor measure) followed the same form. The results show that even in the presence of biospeckle, the OMT trace was recoverable. From this, it is expected that the OMT signal will be measureable from the eye sclera.

The mathematical biospeckle simulated in this work is a first-order empirical model. Rather than attempting to present a complete theoretical model, this model was based on matching the temporal and spatial properties of the simulated speckle with the corresponding properties seen *in vivo*. A limitation of the model presented is that it assumes the speckle scattered from both the surface and volume elements of the media retain the same linear polarization of the incident light. In practice, the volume component would be expected to demonstrate depolarization. The simplified model presented here does, however, capture the interesting aspect of interference between the volume and surface components and models the basic behavior expected using speckle correlation metrology with a volume scatterer. A somewhat higher level model could include a second volume matrix representing the speckle with a polarization orthogonal to that of the surface component and the "parallel" volume component. As the parallel and perpendicular components do not interfere, the net effect would be the addition of static component to each speckle image frame (subjected to the same decorrelation effects modeled for the parallel volume component). The likely impact of this component would be to contribute to bias error in frame-to-frame displacement estimates.

A further limitation of the model is that it is based on results from a small ($n = 3$) number of volunteers. In addition, the model parameters we used were matched empirically to the results seen for a particular optical configuration. At a different wavelength, power, and optical setup, the model parameters used here may not give such a good match to observed speckle. To fully model biospeckle from the sclera would require an in-depth knowledge of the scattering properties of the sclera and of the temporal changes in these properties. A more precise understanding of the physics and statistics of the scattering interaction of these cells with laser light is also required. With a fuller understanding of these properties, other quantities such as the number of scatterers producing biospeckle and the rate of biospeckle could be included into the mathematical model.

The results of this paper show that biospeckle alone does not lead to a significant change in the measured angular displacement. Multiple scattering within the sclera is believed to cause a bias amplitude error but further work is needed to quantify and define the error. Based on the results, it is expected that biospeckle images captured *in vivo* from the sclera will result in an OMT measurement that has a smaller than expected amplitude, due to multiple scattering of the laser light at the sclera, but that the biospeckle activity will be stable enough to track the displacement once a sufficiently high frame rate is used.

5 Conclusions

The aims of this work were (1) to assess how rapidly biospeckle frames from the *in-vivo* eye sclera decorrelate due to the time-dependent biospeckle and (2) to establish if this decorrelation impacts on the feasibility of the proposed speckle correlation technique for OMT measurement.

It was found that decorrelation due to biospeckle was rapid and the method of cross-correlating each frame with an original reference frame is not suitable. To overcome the difficulties associated with biospeckle-induced decorrelation, each biospeckle image frame should be cross correlated with the previous frame. With the frame rate available for this work, the shortest separation between frames was 2 ms.

A mathematical model to simulate biospeckle captured from the eye sclera at a frame rate of 500 Hz was presented and analyzed. The model gave a good qualitative and quantitative match to the speckle patterns seen *in vivo*. In the model, it was found that OMT-like displacements were recoverable from biospeckle images, provided the consecutive images remained "stable" at a level >0.1 dB for the mean peak height-to-floor ratio of the correlation peak. Based on speckle measurements recorded from volunteers in this study, it is expected that if *in-vivo* speckle images are correlated on a frame-to-frame basis, they will fulfil this requirement.

Acknowledgments

This work is based on research supported by Science Foundation Ireland.

References

1. S. Bojanic and C. Bolger, "Ocular microtremor (OMT): a useful indicator of outcome in coma?" *Br. J. Anaesth.* **82**(5), 795P–796P (1999).
2. S. Bojanic, T. Simpson, and C. Bolger, "Ocular microtremor (OMT): a tool for measuring depth of anaesthesia?" *Br. J. Anaesth.* **87**, 364P–365P (2001).
3. C. Bolger et al., "Ocular microtremor in brain stem death," *Neurosurgery* **44**(6), 1201–1206 (1999).
4. C. Bolger et al., "Ocular microtremor (OMT): a new neurophysiological approach to multiple sclerosis," *J. Neurol. Neurosurg. Psychiatry* **68**(5), 639–642 (2000).
5. C. Bolger et al., "Ocular microtremor in patients with idiopathic Parkinson's disease," *J. Neurol. Neurosurg. Psychiatry* **66**(4), 528–531 (1999).
6. C. Bolger et al., "Ocular microtremor in oculomotor palsy," *J. Neuro-Ophthalmol.* **19**(1), 42–45 (1999).
7. D. Coakley and J. Phillips, "Ocular microtremor of patients with brainstem injury," *J. Neurol. Neurosurg. Psychiatry* **47**(10), 1146–1146 (1984).
8. D. Coakley and J. G. Thomas, "Ocular microtremor record and prognosis of unconscious patient," *Lancet* **309**(2), 512–515 (1977).
9. D. Coakley and J. G. Thomas, "The ocular microtremor record as a potential procedure for establishing brain death," *J. Neurol. Sci.* **31** (2), 199–205 (1977).
10. D. Coakley, J. G. Thomas, and J. N. Lunn, "Effect of anesthesia on ocular microtremor," *Br. J. Anaesth.* **48**(11), 1122–1123 (1976).
11. H. Bengi and J. G. Thomas, "Three electronic methods for recording ocular tremor," *Med. Biol. Eng.* **6**(2), 171–178 (1968).
12. N. Sheahan et al., "Ocular microtremor measurement system: design, and performance," *Med. Biol. Eng. Comput.* **31**(3), 205–212 (1993).
13. N. Sheahan, *Ocular Microtremor Measurement Technique and Biophysical Analysis*, PhD Thesis, Trinity College, Dublin (1991).
14. N. F. Sheahan et al., "Sources of variance in ocular microtremor," *Physiol. Measure.* **15**(1), 101–106 (1994).
15. Z. Zhu and Q. Ji, "Eye, and gaze tracking for interactive graphic display," *Mach. Vision Appl.* **15**(3), 139–148 (2004).
16. C. Fagiani, M. Betke, and J. Gips, "Evaluation of tracking methods for human-computer interaction," in *Sixth IEEE Workshop Proc. Applications of Computer Vision*, pp. 121–126, IEEE, (2002).
17. M. Betke, J. Gips, and P. Fleming, "The Camera Mouse: visual tracking of body features to provide computer access for people with severe disabilities," *IEEE Trans. Neural Syst. Rehabil. Eng.* **10**(1), 1–10 (2002).
18. E. Kenny, D. Coakley, and G. Boyle, "Ocular microtremor measurement using laser-speckle metrology," *J. Biomed. Opt.* **18**(1), 016010 (2013).
19. B. Rose, H. Imam, and S. G. Hanson, "Non-contact laser speckle sensor for measuring one-, and two-dimensional angular displacement," *J. Opt.* **29**(3), 115–120 (1998).
20. B. Rose et al., "Laser-speckle angular-displacement sensor: theoretical and experimental study," *Appl. Opt.* **37**(11), 2119–2129 (1998).
21. J. C. Dainty, *Progress in Optics*, Vol. 14, E. Wolf, Ed., Elsevier, Rochester, NY, USA (1976).
22. R. K. Erf, *Speckle Metrology*, Academic Press, Massachusetts, USA (1978).
23. M. Françon, *Laser Speckle and Applications in Optics*, 1st ed., p. 161, Academic Press, New York, USA (1979).
24. J. Goodman, *Laser Speckle and Related Phenomena*, Chapter 2, J. C. Dainty, Ed., pp. 9–75, Springer-Verlag (1975).
25. J. W. Goodman, "Some fundamental properties of speckle." *J. Opt. Soc. Am.* **66**(11), 1145–1150 (1976).
26. R. A. Braga et al., "Reliability of biospeckle image analysis," *Opt. Lasers Eng.* **45**(3), 390–395 (2007).
27. A. Oulamara, G. Tribillon, and J. Duvernoy, "Biological-activity measurement on botanical specimen surfaces using a temporal decorrelation effect of laser speckle," *J. Modern Opt.* **36**(2), 165–179 (1989).
28. H. J. Rabal and R. A. Braga, *Dynamic Laser Speckle, and Applications*, CRC Press, Florida, USA (2008).
29. P. King, "Low level laser therapy: a review," *Lasers Med. Sci.* **4**(3), 141–150 (1989).
30. R. M. Haralick and L. G. Shapiro, *Computer and Robot Vision*, Addison-Wesley Pub. Co., Boston, MA, USA (1993).
31. R. Arizaga, M. Trivi, and H. Rabal, "Speckle time evolution characterization by the co-occurrence matrix analysis," *Opt. Laser Technol.* **31**(2), 163–169 (1999).
32. J. W. Goodman, *Speckle Phenomena in Optics: Theory and Applications*, Roberts & Company Publishers, Colorado, USA (2007).
33. J. D. Briers, "Speckle fluctuations and biomedical optics—implications and applications," *Opt. Eng.* **32**(2), 277–283 (1993).
34. H. J. Rabal, "Numerical model for dynamic speckle: an approach using the movement of the scatterers," *J. Opt. A Pure Appl. Opt.* **5**(5), S381–385 (2003).
35. A. Federico et al., "Simulation of dynamic speckle sequences and its application to the analysis of transient processes," *Opt. Commun.* **260**(2), 493–499 (2006).
36. Photometrics, Photometrics, Arizona, http://www.photometrics.com (2010).
37. MATLAB version R2009a, The MathWorks Inc., Natick, Massachusetts (2010).
38. D. D. Duncan and S. J. Kirkpatrick, "The copula: a tool for simulating speckle dynamics," *J. Opt. Soc. Am. A* **25**(1), 231–237 (2008).
39. M. Al-Kalbani, *Ocular Microtremor Measurement, Characterization & Analysis*, PhD Thesis, Trinity College, University of Dublin, Dublin (2009).
40. N. Collins, *Ocular Microtremor as a Clinical and Scientific Tool in Neurologic Disease; Validation and Application of a Generalized Discovery Protocol*, PhD Thesis, University of Dublin, Trinity College, Dublin (2011).
41. M. Weeks, *Digital Signal Processing Using MATLAB & Wavelets*, 2nd ed., Jones & Bartlett Learning, Massachusetts, USA (2011).